Diffusive instabilities in a hyperbolic activator-inhibitor system with superdiffusion

Alain Mvogo,[1,2,*] Jorge E. Macías-Díaz,[3,†] and Timoléon Crépin Kofané[4,‡]

[1]*Laboratory of Biophysics, Department of Physics, Faculty of Science, University of Yaounde I, P.O. Box 812, Cameroon*
[2]*Abdus Salam International Center For Theoretical Physics, P.O. Box 586, Strada Costiera 11, 34014 Trieste, Italy*
[3]*Departamento de Matemáticas y Física, Universidad Autónoma de Aguascalientes, Avenida Universidad 940, Ciudad Universitaria, Aguascalientes, Aguascalientes 20131, Mexico*
[4]*Laboratory of Mechanics, Department of Physics, Faculty of Science, University of Yaounde I, P.O. Box 812, Cameroon*

(Received 2 January 2018; revised manuscript received 1 March 2018; published 23 March 2018)

We investigate analytically and numerically the conditions for wave instabilities in a hyperbolic activator-inhibitor system with species undergoing anomalous superdiffusion. In the present work, anomalous superdiffusion is modeled using the two-dimensional Weyl fractional operator, with derivative orders $\alpha \in [1,2]$. We perform a linear stability analysis and derive the conditions for diffusion-driven wave instabilities. Emphasis is placed on the effect of the superdiffusion exponent α, the diffusion ratio d, and the inertial time τ. As the superdiffusive exponent increases, so does the wave number of the Turing instability. Opposite to the requirement for Turing instability, the activator needs to diffuse sufficiently faster than the inhibitor in order for the wave instability to occur. The critical wave number for wave instability decreases with the superdiffusive exponent and increases with the inertial time. The maximum value of the inertial time for a wave instability to occur in the system is $\tau_{\max} = 3.6$. As one of the main results of this work, we conclude that both anomalous diffusion and inertial time influence strongly the conditions for wave instabilities in hyperbolic fractional reaction-diffusion systems. Some numerical simulations are conducted as evidence of the analytical predictions derived in this work.

DOI: 10.1103/PhysRevE.97.032129

I. INTRODUCTION

Different processes in dendritic and population growth, fluid dynamics, pulse propagation in nerves, and many other biological, chemical, and physical phenomena have been found to be well described by reaction-diffusion equations. In their standard form, those models are partial differential equations of the parabolic type [1], where perturbations propagate infinitely fast in the medium. In these systems, waves and spatiotemporal patterns arise at the onset of an instability of the steady state. However, there exists a range of applications lacking a satisfactory description of the spatial dispersion through simple diffusive transport.

It is well known that the diffusion equation possesses the undesirable feature that localized disturbances spread infinitely fast through the system, although with heavy attenuation. This pathology of the diffusion equation stems from a lack of inertia of particles. On the other hand, hyperbolic reaction-transport equations (which are a means to describe transport with inertia) provide physically acceptable models of biological, physical, and chemical systems [2–8]. Moreover, an important and often overlooked assumption in reaction-diffusion models is the use of the classical Laplacian operator for the description of transport. The use of this operator is motivated by the Fourier-Fick model, according to which the flux is assumed to be proportional to the gradient of the concentration. From the statistical mechanics point of view, this prescription is linked to the assumption that the underlying "microscopic" transport process is driven by an uncorrelated Markovian, Gaussian process. However, despite its relative success, experimental, numerical, and theoretical evidence indicate that the standard diffusion models have limited applicability. For instance, some reports reveal that the morphogen diffusion in living cell environments is non-Fickian and it certainly does not satisfy the standard reaction-diffusion system model [9]. Therefore, a problem of considerable interest is the study of the role of anomalous diffusion (Lévy flights, in particular) in reaction-diffusion models.

Anomalous diffusion is also inherent to certain plasma systems [10] and heterogeneous solid state materials [11,12] among other models. One of the most studied types of anomalous diffusion is superdiffusion, which is a process that is faster than normal diffusion. Superdiffusion corresponds to a jump size distribution having infinite moments or, alternatively, to Lévy flights [13]. The effects of superdiffusion on pattern formation and pattern selection have been explored in the substrate-depleted Brusselator model [14]. The results have revealed that Turing instabilities can occur even when the diffusion of the inhibitor is slower than that of the activator. Zhang and Tian [15] investigated the effects of superdiffusion on Turing instabilities in an activator-inhibitor system describing the chlorite-iodine-malonic acid reaction [16]. They found that Turing patterns emerge when the ratio of the anomalous diffusion exponent of the inhibitor with respect to that of the activator is much smaller than unity. However, the investigation of wave instabilities in hyperbolic activator-inhibitor systems with superdiffusion remains unexplored.

*mvogal_2009@yahoo.fr
†jemacias@correo.uaa.mx
‡tckofane@yahoo.com

It is worthwhile to recall that the analytical determination of parametric conditions under which distinctive patterns are generated in reaction-diffusion systems has been an interesting avenue of research in recent years. As an example, the development of morphogen gradients with spatially varying degradation rates was recently studied in the literature [17]. Different pattern configurations have been examined in the context of reaction-diffusion systems. For instance, some recent works report on the hyperbolic chaos of Turing patterns [18] and the statistical properties of growth rates of a linear oscillator driven by parametric noise [19]. Moreover, various applications of reaction-diffusion processes with active particles have been recently proposed, like some analytical reports on giant polymer diffusivity in crowded solutions of active particles [20].

In this paper we investigate the conditions for the occurrence of diffusion-driven wave instabilities in a hyperbolic version of the fractional model investigated in [15]. In Sec. II we present the hyperbolic fractional model of interest. Moreover, we carry out therein a linear stability analysis of the uniform steady state to determine the conditions for diffusion-driven wave instabilities. In turn, Secs. III and IV are devoted to provide analyses of Turing and wave instabilities, respectively. In Sec. V we describe briefly the numerical method to approximate the solutions of the model under investigation. Some numerical simulations are carried out then to verify the validity of the analytical predictions. A summary is given and some conclusions are discussed in Sec. VI.

II. MODEL AND LINEAR STABILITY ANALYSIS

In this work we investigate the following hyperbolic activator-inhibitor model with superdiffusion consisting of two variables:

$$\tau_u \frac{\partial^2 u}{\partial t^2} + \frac{\partial u}{\partial t} = u - av + buv - u^3 + \nabla^\alpha u,$$
$$\tau_v \frac{\partial^2 v}{\partial t^2} + \frac{\partial v}{\partial t} = u - cv + d\nabla^\alpha v. \tag{1}$$

Here the positive constants $\tau_{u,v}$ are inertial times and d is the diffusion ratio between the inhibitor u and activator v. The reaction terms in (1) were first proposed by Dufiet and Boissonade to describe the chlorite-iodine-malonic acid reaction [16]. In this model the cubic term $-u^3$ limits the exponential growth of the perturbation and allows for the saturation of the instability. Meanwhile, the quadratic term buv avoids the invariance in the transformation $(u,v) \to (-u,-v)$, which is nongeneric in chemical systems. The parameters a, b, and c are positive constants and the superdiffusion is described by the Weyl fractional operator ∇^α of order α with $1 \leqslant \alpha \leqslant 2$ [21]. In one dimension, the Weyl fractional operator is given by

$$\nabla^\alpha w = -c_\alpha \left({}_{-\infty}D_x^\alpha w + {}_x D_{+\infty}^\alpha w \right), \tag{2}$$

where w stands for u or v. Moreover,

$$c_\alpha = \frac{1}{2\cos(\alpha\pi/2)}, \tag{3}$$

$${}_{-\infty}D_x^\alpha w = \frac{1}{\Gamma(2-\alpha)} \frac{d^2}{dx^2} \int_{-\infty}^{x} \frac{w(\zeta,t)}{(x-\zeta)^{\alpha-1}} d\zeta, \tag{4}$$

$${}_x D_{+\infty}^\alpha w = \frac{1}{\Gamma(2-\alpha)} \frac{d^2}{dx^2} \int_{x}^{+\infty} \frac{w(\zeta,t)}{(\zeta-x)^{\alpha-1}} d\zeta, \tag{5}$$

where $\Gamma(z) = \int_0^{+\infty} t^{z-1} e^{-t} dt$ is the Gamma function, which is the generalization of the factorial representations $\Gamma(n+1) = n! = n \times (n-1) \times (n-2) \times \cdots \times 1$ $(n \in \mathbb{N})$ used in conventional vector calculus.

The equivalent definition in Fourier space allows for a simple generalization of the fractional operator to several spatial dimensions. Recall that $\mathcal{F}(\nabla^\alpha w) = -|k|^\alpha \mathcal{F}(w)$ is satisfied in one spatial dimension. For the higher-dimensional scenario, the Laplacian is replaced by the operator $\nabla^\alpha = -(-\nabla)^{\alpha/2}$, defined by its action in Fourier space as $\mathcal{F}(\nabla^\alpha w) = -\|\mathbf{k}\|^\alpha \mathcal{F}(w)$. This definition serves as a good continuous model of a random walk describing Lévy flights, as it correctly captures the asymptotic behavior of a particle probability to perform long jumps. System (1) proposes a suitable description of a reactive system where the medium enables enhanced diffusion of Lévy flight type, while each species' exponent is determined by its own mobility properties.

The system (1) is presented here in a dimensionless form. The purpose of studying this scaled model is to determine its analytical features in the simplest possible scenario. We refer here to [16] for the study of the motivating model. It is important to point out that scaled systems with dimensionless quantities are usually investigated in the sciences in order to capture their essential analytical properties [15,16]. In particular, the investigation of dimensionless models has led to the identification of similar distinctive features in the Schnackenberg model [22,23] or the Brussellator [24]. It is worth pointing out that this approach has been followed not only for reaction-diffusion systems, but also for the investigation of diffusive patters in hyperbolic models [8].

The hyperbolic fractional system (1) has three spatially uniform stationary states (USSs) $(u_0,v_0) = (0,0)$, $(u_1,v_1) = (A_+,B_+)$, and $(u_2,v_2) = (A_-,B_-)$, where

$$A_\pm = \frac{b \pm \sqrt{b^2 + 4c(c-a)}}{2c}, \tag{6}$$

$$B_\pm = \frac{b \pm \sqrt{b^2 + 4c(c-a)}}{2c^2}. \tag{7}$$

When b is small, it is assumed that the last two equilibria exist only when the first equilibrium surpasses by far the Turing bifurcation point. Thus we can ignore the existence of the latter two equilibria. In this paper we only analyze the stability of the equilibrium (u_0,v_0).

In the absence of diffusion and inertia, the spatially homogeneous system associated with (1) exhibits a Hopf bifurcation at $c = 1$ when $a > 1$. The equilibrium is stable with respect to any small spatially homogeneous perturbation for $1 < c < a$. In the presence of both diffusion and inertia, to determine the stability of the USS with respect to spatially nonuniform perturbations, we write $u(\mathbf{r},t)$ and $v(\mathbf{r},t)$ as

$$u(\mathbf{r},t) = u_0 + \varepsilon \Delta u + \text{c.c.} + O(\varepsilon^2), \tag{8}$$

$$v(\mathbf{r},t) = u_0 + \varepsilon \Delta v + \text{c.c.} + O(\varepsilon^2), \tag{9}$$

where the perturbations Δu and Δv depend on both space and time and $\mathbf{r}$ is the spatial vector.

Substituting (8) and (9) into (1) and then linearizing, we obtain the system

$$\tau_u \frac{\partial^2 \Delta u}{\partial t^2} + \frac{\partial \Delta u}{\partial t} = J_{11}\Delta u + J_{12}\Delta v + \nabla^\alpha u,$$
$$\tau_v \frac{\partial^2 \Delta v}{\partial t^2} + \frac{\partial \Delta v}{\partial t} = J_{21}\Delta u + J_{22}\Delta v + d\nabla^\alpha v, \quad (10)$$

where J_{11}, J_{12}, J_{21}, and J_{22} are the components of the associated Jacobian matrix. Here we assume that the perturbations Δu and Δv are superpositions of normal modes, that is,

$$\Delta u = C_u \exp(\lambda t + i\mathbf{k}\cdot\mathbf{r}), \quad (11)$$

$$\Delta v = C_v \exp(\lambda t + i\mathbf{k}\cdot\mathbf{r}). \quad (12)$$

The parameters C_u and C_v are constants, λ is the growth rate of the perturbation at the time t, $\mathbf{k}$ is the wave vector, and $i^2 = -1$. According to the definition of the Weyl fractional operator ∇^α, we readily obtain the matrix equation

$$\begin{pmatrix} D_1 & -a \\ 1 & D_2 \end{pmatrix}\begin{pmatrix} C_u \\ C_v \end{pmatrix} = 0, \quad (13)$$

where the diagonal entries of the 2×2 matrix on the left-hand side of this identity are defined by

$$D_1 = 1 - \tau_u\lambda^2 - \lambda - k^\alpha, \quad (14)$$

$$D_2 = -c - \tau_v\lambda^2 - \lambda - dk^\alpha. \quad (15)$$

Moreover, the number $k = \|\mathbf{k}\|$ is the Euclidean norm of the wave vector of the perturbation.

The matrix identity (13) has a nontrivial solution only if the determinant of the matrix is equal to zero. This leads to a quartic equation in λ for which the form of its roots is rather complicated. For simplification purposes, we introduce the variables

$$\beta_1 = 1 - k^\alpha, \quad (16)$$

$$\beta_2 = -c - dk^\alpha. \quad (17)$$

To further simplify the analysis, we define

$$\gamma_{u,v} \equiv \tau_{u,v}\lambda^2 + \lambda \quad (18)$$

and assume that $\tau_u = \tau_v \equiv \tau$. Under these circumstances, notice that $\gamma_u = \gamma_v \equiv \gamma$. This leads to the biquadratic equation

$$\gamma^2 - (\beta_1 + \beta_2)\gamma + \beta_1\beta_2 + a = 0, \quad (19)$$

where

$$\gamma \equiv \tau\lambda^2 + \lambda. \quad (20)$$

In turn, the roots of (19) lead to the following eigenvalues governing the stability of the USS:

$$\lambda_{1,2} = -\frac{1}{2\tau} \pm \sqrt{\frac{1}{4\tau^2} + \frac{\gamma_1}{\tau}}, \quad (21)$$

$$\lambda_{3,4} = -\frac{1}{2\tau} \pm \sqrt{\frac{1}{4\tau^2} + \frac{\gamma_2}{\tau}}, \quad (22)$$

where

$$\gamma_{1,2} = \frac{\beta_1 + \beta_2}{2} \pm \sqrt{\left(\frac{\beta_1 - \beta_2}{2}\right)^2 - a}. \quad (23)$$

The expressions (23) will be used in this work to explore the features of the diffusive instabilities in the hyperbolic fractional system (1).

Before closing this section, it is important to mention that the use of the perturbation expansion considered here has some inherent limitations. For example, it is only valid for disturbances which are initially small, though we must recall that such an analytical approach has been followed already in various reports [8,25,26]. However, this approach has also some virtues. For instance, small-amplitude perturbations that grow spontaneously provide a natural explanation for the existence of finite-amplitude fluctuations. This is justified by the fact that small-background fluctuations are always present to act as seeds for the instabilities. On the other hand, dealing with small perturbations reduces the question to the stability properties of the basic flow and not to the amplitude level of the perturbations. If the perturbations were large (as large as the basic flow) it could be difficult to understand what one means by instability. Finally, small-amplitude perturbations must get their energy directly from the basic flow, while large-amplitude perturbations could get energized by the interaction with the ultimate energy source through other perturbations.

III. TURING INSTABILITY

For Turing instabilities to occur in (1), the eigenvalues of the system must be real and have a positive maximum at the wave number $k_T > 0$. Turing bifurcation occurs then when $\mathrm{Im}\,\lambda_n = \mathrm{Re}\,\lambda_n = 0$ $(n = 1,2,3,4)$ at $k = k_T \neq 0$. The onset of the diffusion-driven instability determining the critical values of the control parameter and the critical wave number corresponds to $\lambda_n = d\lambda_n/dk = 0$. An analysis of (1) reveals that the USS (u_0,v_0) undergoes a Turing instability for the critical wave number k_T and the parameter value a_T given by

$$k_T = \left(\frac{d-c}{2d}\right)^{1/\alpha}, \quad (24)$$
$$a_T = \frac{(d+c)^2}{4d}. \quad (25)$$

At the Turing bifurcation threshold, the spatial symmetry of the system is broken and the patterns are stationary in time and oscillatory in space with the corresponding wavelength $\lambda_T = 2\pi/k_T$.

It is well known that in standard reaction-diffusion systems, Turing bifurcation requires activator-inhibitor kinetics (that is, $J_{11} > 0$ and $J_{22} < 0$) and the inhibitor needs to diffuse sufficiently faster than the activator. This imposes on the hyperbolic fractional system (1) the condition $d > 1$. As expected, we also have $J_{11} = 1 > 0$ and $J_{22} = -c < 0$, so the following parameter space is required for Turing instabilities:

$$1 < c < a < a_T, \quad d > 1, \quad b < \sqrt{c(a-c)}. \quad (26)$$

Note that these conditions are independent of the inertial time τ and are similar to those obtained in [15]. We conclude that stationary bifurcations are not affected by inertia in

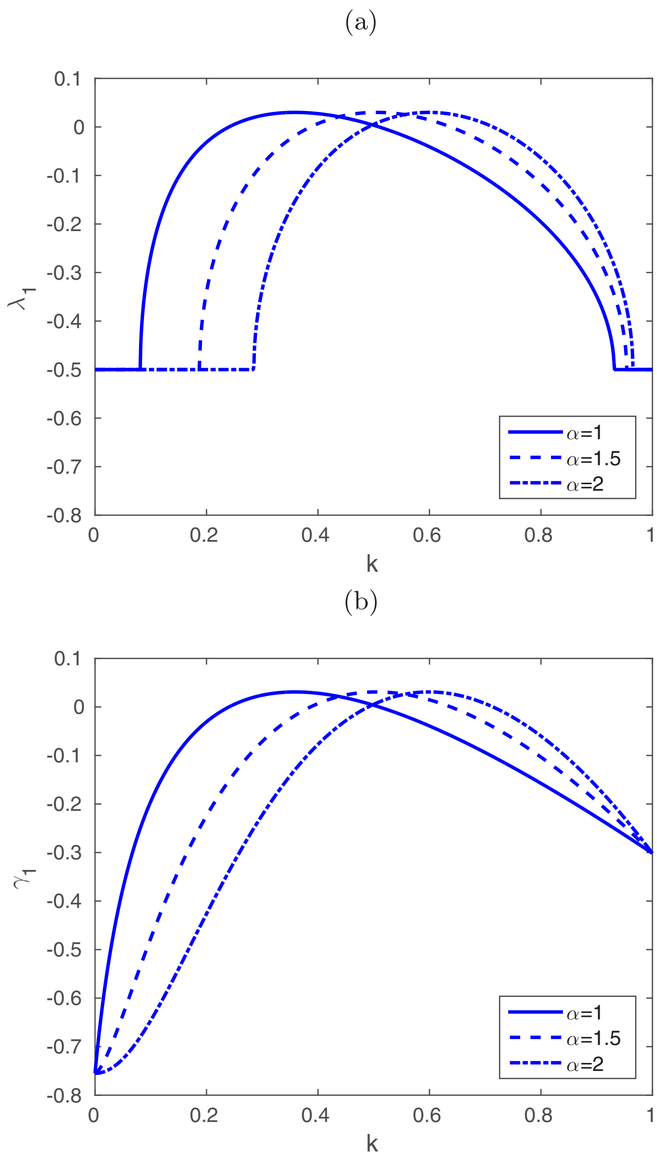

FIG. 1. Dispersion curves for the real eigenvalues (a) λ_1 and (b) γ_1 for $\alpha = 1$ (solid lines), $\alpha = 1.5$ (dashed lines), and $\alpha = 2$ (dash-dotted lines). The graphs were obtained using the expressions (21) and (23), respectively, with $a = 7.45$, $b = 2.5$, $c = 5$, $d = 20$, and $\tau = 1$.

the transport. Moreover, the Turing instability conditions are identical for both hyperbolic and parabolic fractional systems.

Let $a = 7.45$, $b = 2.5$, $c = 5$, $d = 20$, and $\tau = 1$. Figures 1(a) and 1(b) show the behavior of the real eigenvalues λ_1 and γ_1, respectively, as functions of the wave number k for three different orders of differentiation, namely, $\alpha = 1$ (solid line), $\alpha = 1.5$ (dashed line), and $\alpha = 2$ (dash-dotted line). The variation of the eigenvalues λ_1 is compared with γ_1, which is the eigenvalue of the parabolic form of (1). Clearly, for each value of the superdiffusive exponent α, the eigenvalues of both the parabolic and the hyperbolic fractional systems change sign at the Turing instability point with the same critical values a_T and k_T. At the onset of the Turing instability, both curves $\lambda_1(k)$ and $\gamma_1(k)$ touch the k axis at the same point, as expected from the identity (20). The active wave number k is affected by the superdiffusive exponent α. Indeed, k increases with α.

IV. WAVE INSTABILITY

For the wave instability to occur in (1), all the eigenvalues must satisfy $\mathrm{Im}\,\lambda_n \neq 0$. Equivalently,

$$\left(\frac{\beta_1 - \beta_2}{2}\right)^2 - a < 0. \tag{27}$$

The complex eigenvalues have positive real parts for some range of k and exhibit a maximum of $\mathrm{Re}\,\lambda_n$ at some finite k_{w}. The onset of the diffusion-driven wave instability corresponds to $\mathrm{Re}\,\lambda_n = 0$, with $k \neq 0$ and $\frac{d\,\mathrm{Re}\,\lambda_n}{dk} = 0$. So we can write the eigenvalues in the complex form [8]

$$\lambda_{1,2} = -\frac{1}{2\tau} \pm y \pm iz, \tag{28}$$

$$\lambda_{3,4} = -\frac{1}{2\tau} \pm y \mp iz, \tag{29}$$

where $\mathrm{Re}\,\lambda_n = -\frac{1}{2\tau} \pm y$ and $\mathrm{Im}\,\lambda_n = \pm z$ are such that

$$y = \sqrt{\tfrac{1}{2}\left(\sqrt{n_{1\tau}^2 + n_{2\tau}^2} + n_{1\tau}\right)}, \tag{30}$$

$$z = \sqrt{\tfrac{1}{2}\left(\sqrt{n_{1\tau}^2 + n_{2\tau}^2} - n_{1\tau}\right)} \tag{31}$$

and

$$n_{1\tau} \equiv \frac{1}{4\tau^2} + \frac{1}{\tau}\left(\frac{\beta_1 + \beta_2}{2}\right), \tag{32}$$

$$n_{2\tau} \equiv \frac{1}{\tau}\sqrt{a - \frac{(\beta_1 - \beta_2)^2}{4}}. \tag{33}$$

The sign of the real part can change only for the eigenvalues $\lambda_{1,3} = -\frac{1}{2\tau} + y \pm iz$. The onset of the diffusion-driven wave instability corresponds to $y = \frac{1}{2\tau}$ and $\frac{dy}{dk} = 0$, and $\mathrm{Re}\,\lambda_n$ for $k = 0$.

Note that the boundary between the real and complex eigenvalues is described by

$$k^\alpha(1 - d) = 1 + c \mp 2\sqrt{a}, \tag{34}$$

which determines the zero-value curves or nullclines in parameter space. Let

$$h_\alpha^\pm(k,a) = 1 + c \pm 2\sqrt{a} - k^\alpha(1 - d) = 0. \tag{35}$$

With this convention, Fig. 2 shows the nullclines $h_\alpha^-(k,a)$ corresponding to three different values of the superdiffusive exponent, namely, $\alpha = 1$ (solid line), $\alpha = 1.5$ (dashed line), and $\alpha = 2$ (dash-dotted line). Figure 2(a) shows that if $d = 20$ (in which case $d > 1$), there exist intervals of a where the eigenvalues λ are real for the whole range of k. In contrast, Fig. 2(b) shows that if $d = 0.25$ (that is, $d < 1$), for any value of the control parameter a, intervals of the wave number k where the eigenvalues λ are real ($h_\alpha^- > 0$) and intervals where the eigenvalues are complex ($h_\alpha^- < 0$) coexist.

As a consequence of these findings, a Turing instability in the parabolic form of (1) can occur only if $d > 1$, and the Turing conditions coincide for both hyperbolic and parabolic fractional systems (1). Figure 2 also shows the important role of the superdiffusion exponent α in the nullclines $h_\alpha^\pm(k,a) = 0$. Moreover, Fig. 2(a) shows that the domain of k for which the

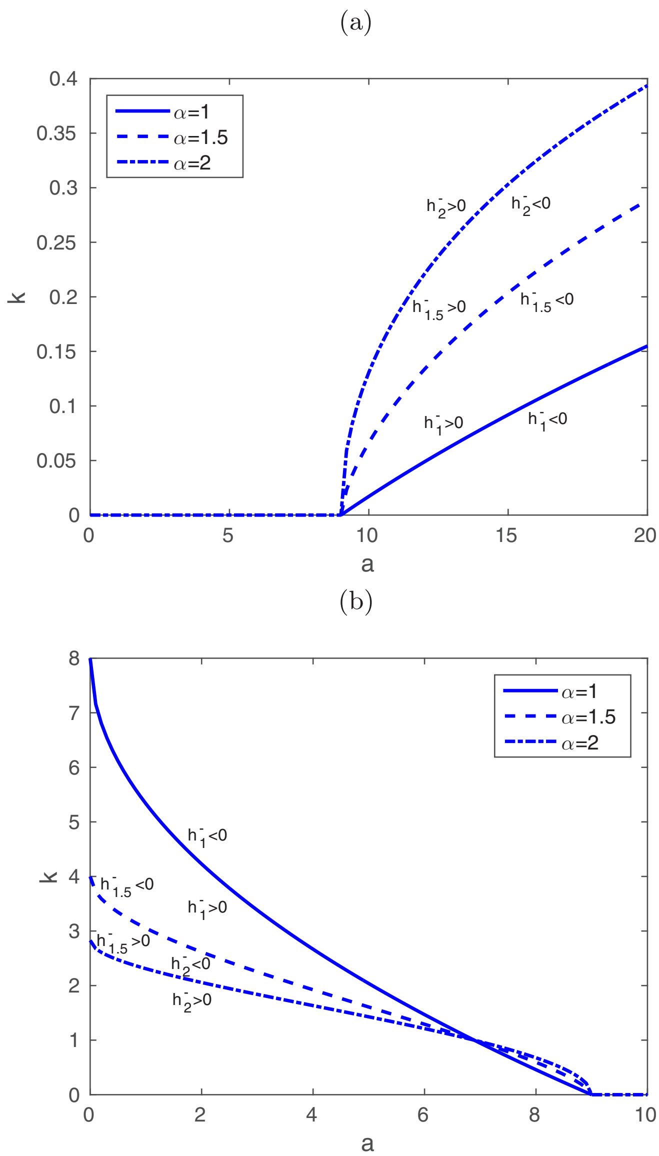

FIG. 2. Diagram of wave number k versus the control parameter a for the hyperbolic fractional Dufiet-Boissonade model with fixed $b = 2.5$, $c = 5$, and $\tau = 1$. We employed (a) $d = 20$ and (b) $d = 0.25$. The curves represent the nullcline equation $h_\alpha^- \equiv h_\alpha^-(k,a) = 0$ using (35) with $\alpha = 1$ (solid line), $\alpha = 1.5$ (dashed line), and $\alpha = 2$ (dash-dotted line).

eigenvalues λ are real decreases when α increases. In contrast, Fig. 2(b) shows that, as α increases, so does the domain of values of k for which the eigenvalues are both real and complex.

The system is at the Hopf bifurcation point of the USS when the mode $k = 0$ has a purely imaginary eigenvalue, that is, when $\lambda(k = 0) = i\omega_H$ with $\omega_H \in \mathbb{R}^+$. Using (19), if the imaginary part vanishes then

$$\omega_H^2 = -\frac{T}{2\tau}, \tag{36}$$

where $T = 1 - c$. As a consequence, the identity (36) requires that $c \geqslant 1$. Moreover, she stability condition for system (1) is given by

$$1 - c < T_H, \quad a - c > 0, \tag{37}$$

where

$$T_H = \frac{1}{\tau}[1 - \sqrt{1 + 4\tau^2(a - c)}]. \tag{38}$$

This equation implies that the USS undergoes a Hopf bifurcation when $k_H = 0$ and

$$a_H = \frac{1}{4\tau^2}[(1 - \tau + \tau c)^2 - 1] + c. \tag{39}$$

The critical value for the Turing instability must be less than that for the Hopf instability, that is,

$$a_T < a_H. \tag{40}$$

Obviously, this will be the case for sufficiently large values of d. Then the Turing instability occurs first in the system as a is increased. For the parameter values $c = 5$, $b = 2.5$, $d = 20$, $\tau = 1$, and $\alpha = 2$, the Hopf condition (39) yields $a_H = 11$ with $\omega_H = 2$ and the Turing condition (26) yields $a_T = 7.8125$ and $k_T = \sqrt{2}/2$. As required, the critical value a_T is less than the critical value a_H, so the Turing instability occurs before the Hopf bifurcation.

As a consequence of the fact that $T < T_H \leqslant 0$, the activator diffuses sufficiently faster than the inhibitor. That is, $1/d \geqslant \Theta_\mathrm{w}$, where Θ_w is the minimum ratio of the diffusion coefficients of the activator and the inhibitor needed for the occurrence of a wave instability, contrary to the requirement for a Turing bifurcation. The wave instability occurs when the real part of an eigenvalue with $k \neq 0$ vanishes. The condition for this instability is obtained by assuming $\lambda(k \neq 0) = i\omega_\mathrm{w}$. Inserting this relation into (19) and separating the real and the imaginary parts, we obtain, respectively,

$$\omega_\mathrm{w}^2 = \frac{(1 + d)k^\alpha - (1 - c)}{2\tau} \tag{41}$$

and

$$\sigma_0 k^{2\alpha} + \sigma_2 k^\alpha + \sigma_4 = 0, \tag{42}$$

where

$$\sigma_0 = (1 - d)^2, \tag{43}$$

$$\sigma_2 = -2\left(1 - c - \frac{1}{\tau}\right)(1 + d) + 4(d - c), \tag{44}$$

$$\sigma_4 = (1 - c)^2 - \frac{2}{\tau}(1 - c) - 4(a - c). \tag{45}$$

For (41) and (42) to hold, the conditions $1 - c \leqslant (1 + d)k^\alpha$ and $\sigma_2 < 0$ are required, respectively.

Figure 3 shows the frequency as a function of the wave number k for the usual values of the superdiffusive exponent α. In all these cases, the frequency is an increasing function of k and the three curves coincide at the same value $k = 1$. For $k < 1$, the frequency increases when α decreases and the frequency increases with α for $k > 1$.

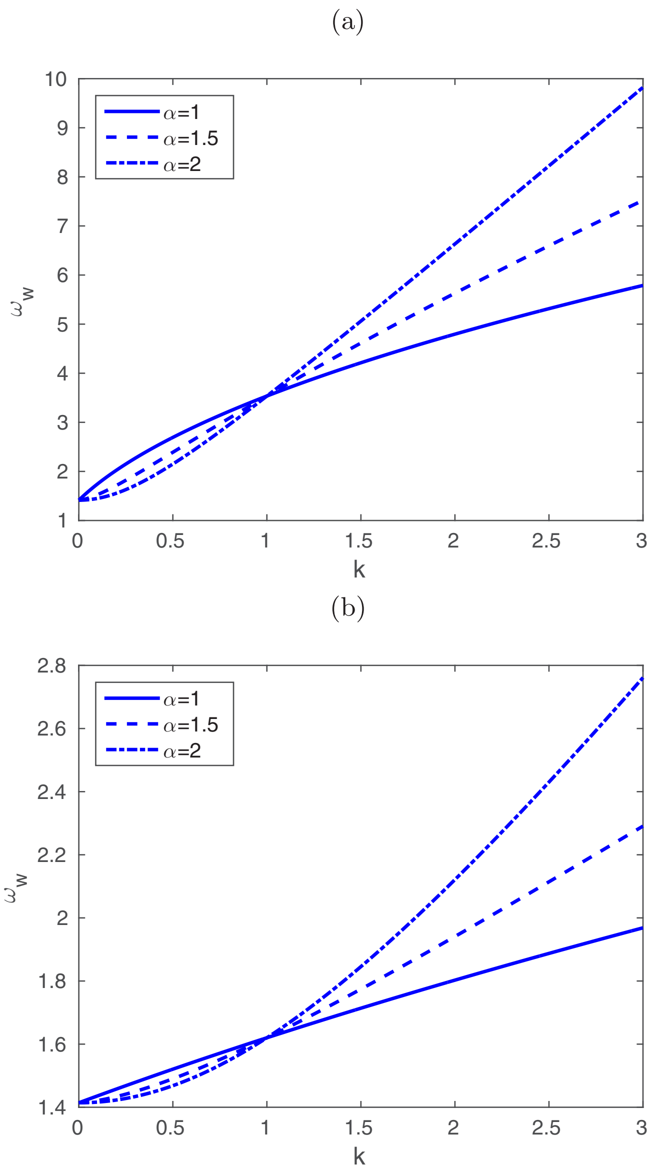

FIG. 3. Frequency of the wave instability for the values $\alpha = 1$ (solid line), $\alpha = 1.5$ (dashed line), and $\alpha = 2$ (dash-dotted line). The graphs were obtained using the expression (41) with $b = 2.5$, $c = 5$, and (a) $d = 20$ and (b) $d = 0.25$.

We solve (42) by setting $k^\alpha = K$. As a result, we obtain the roots

$$K_{1,2} = \frac{-\sigma_2 \pm \sqrt{\sigma_2^2 - 4\sigma_0\sigma_4}}{2\sigma_0}. \tag{46}$$

A wave instability occurs when (42) has a degenerate or double root. The USS of system (1) undergoes a wave instability when the parameter values satisfy

$$\sigma_2^2 - 4\sigma_0\sigma_4 = 0 \tag{47}$$

and the critical wave number is given by

$$k_{\mathrm{w}} = \left(-\frac{\sigma_2}{2\sigma_0}\right)^{1/\alpha}. \tag{48}$$

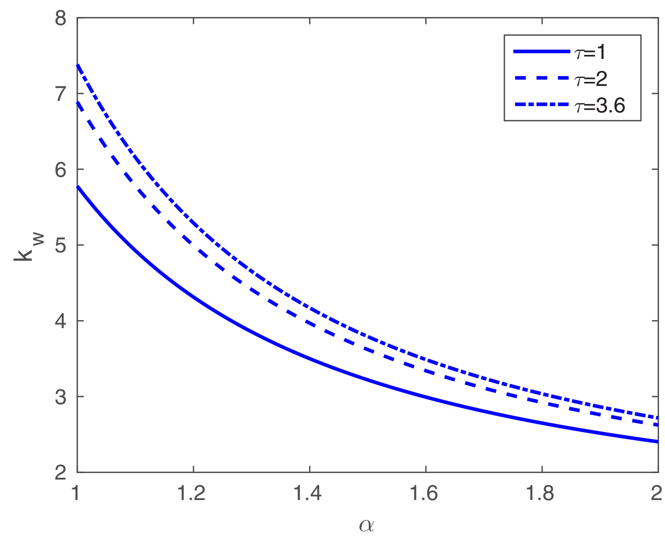

FIG. 4. Critical wave number k_{w} as a function of the superdiffusive exponent α for the values $\tau = 1$ (solid line), $\tau = 2$ (dashed line), and $\tau = 3.6$ (dash-dotted line). The graphs were obtained using the expression (48) with $c = 5$ and $d = 0.25$.

At the wave threshold, the patterns are oscillatory in space and time with the wavelength $\lambda_{\mathrm{w}} = 2\pi/k_{\mathrm{w}}$. Figure 4 shows the dependence of the critical wave number k_{w} on the superdiffusive exponent α, using $c = 5$, $d = 0.25$, and various values of the inertial time, namely, $\tau = 1$ (solid line), $\tau = 2$ (dashed line), and $\tau = 3.6$ (dash-dotted line). Note that k_{w} decreases as α increases. The minimum value of the critical wave number is obtained for $\alpha = 2$, that is, in the case of a normal diffusion. Figure 4 also shows that the amplitude of the critical wave number increases when the inertial time τ increases.

Consider the parameter values $c = 5$, $b = 2.5$, $d = 0.25$, and $\tau = 1$. We calculate the wave instability conditions for three different values of superdiffusive exponent α. We obtain the following critical values of the wave number: $k_{\mathrm{w}} = 5.7778$ for $\alpha = 1$, $k_{\mathrm{w}} = 3.2199$ for $\alpha = 1.5$, and $k_{\mathrm{w}} = 2.4037$ for $\alpha = 2$. For all these different values of α, we obtain the critical values $a_{\mathrm{w}} = 6.3055$ and $\omega_{\mathrm{w}} = 2.3688$ of the control parameter and the frequency of the wave instability, respectively. This information is summarized in Table I for the sake of convenience. As required, the critical value a_{w} is less than the critical value a_H, so the wave instability occurs before the Hopf bifurcation. The intersection of the curves $\mathrm{Re}\,\lambda_{1,3} = 0$ and $\frac{d\,\mathrm{Re}\,\lambda_{1,3}}{dk} = 0$ corresponds to the wave bifurcation point with the critical values a_{w} and k_{w}.

The onset of the wave instability for different values of the superdiffusive exponent α are shown in Fig. 5 for $\alpha = 1$

TABLE I. Critical values of the control parameter a and the wave number for different values of α, namely, 1, 1.5, and 2.

α	a_{w}	k_{w}
1	6.3055	5.7778
1.5	6.3055	3.2199
2	6.3055	2.4037

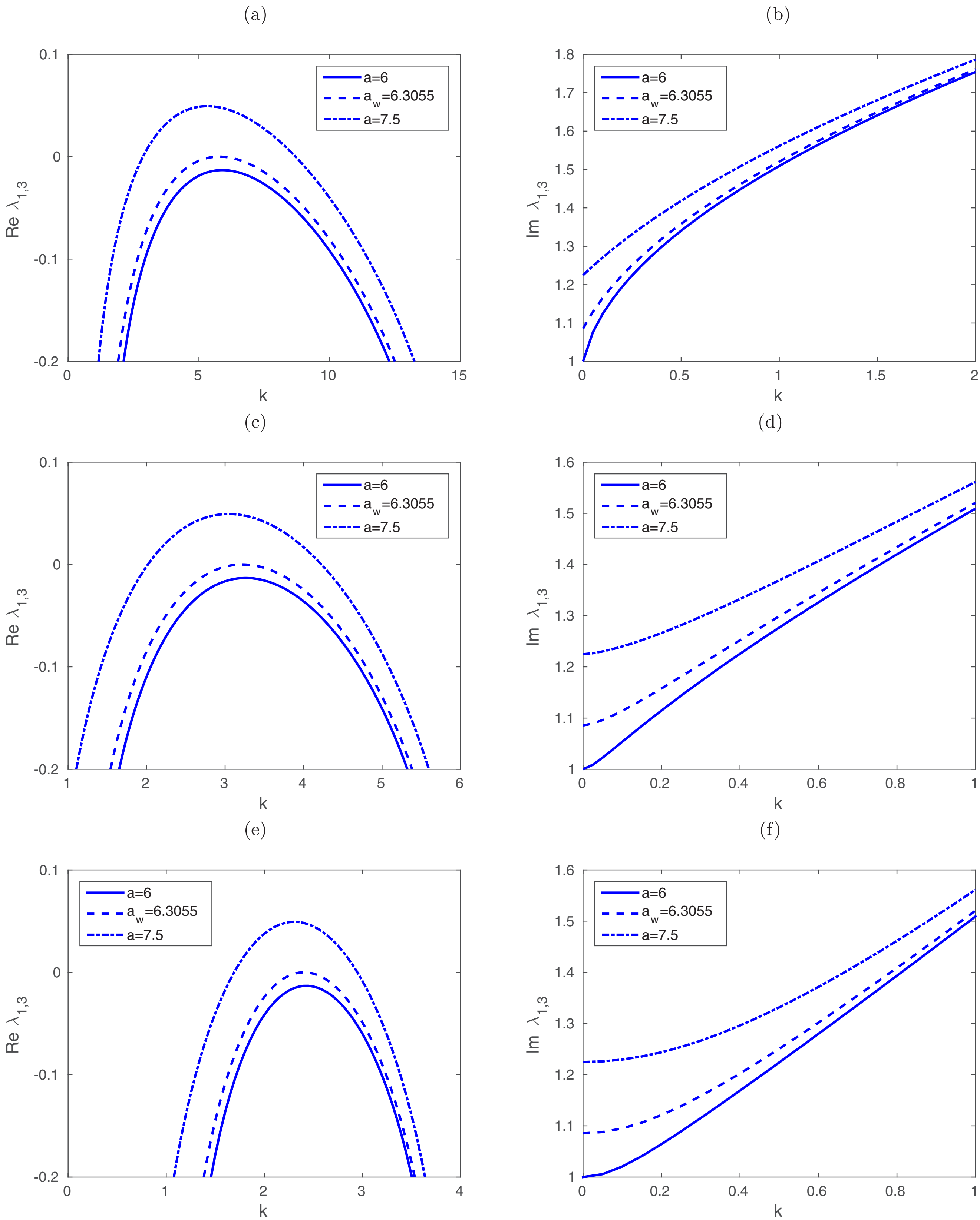

FIG. 5. Dispersion curves for (a), (c), and (e) the real and (b), (d), and (f) the imaginary parts of $\lambda_{1,3}$ as given by $\mathrm{Re}\,\lambda_{1,3} = -1/2\tau + y$ and $\mathrm{Im}\,\lambda_{1,3} = z$, respectively. We considered various values of the differentiation parameter, namely, (a) and (b) $\alpha = 1$, (c) and (d) $\alpha = 1.5$, and (e) and (f) $\alpha = 2$. Various scenarios of the control parameter a were used: before the wave bifurcation ($a = 6$), at the bifurcation point ($a_{\mathrm{w}} = 6.3055$ and $k_{\mathrm{w}} = 5.7778$), and beyond the wave bifurcation point ($a = 7.5$). The critical value for the Hopf bifurcation is $a_H = 11$ and the model parameters were fixed as $c = 5$, $b = 2.5$, $d = 0.25$, and $\tau = 1$.

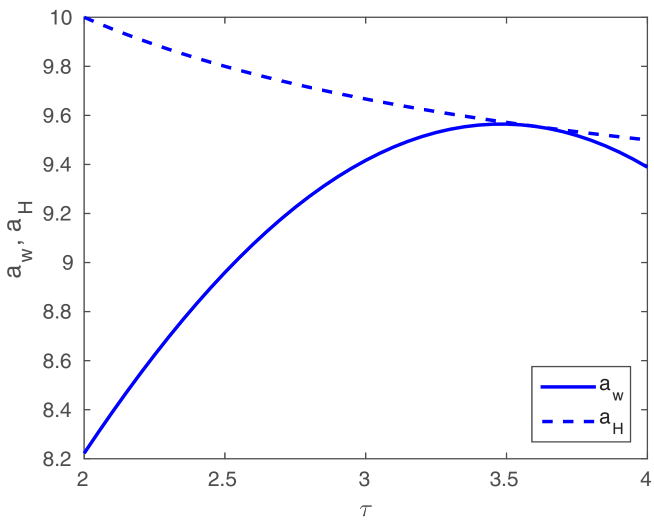

FIG. 6. Both sides of equation $a_H = a_w$ as a function of the inertial time τ, using $b = 2.5$, $c = 5$, and $D = 0.25$.

[Figs. 5(a) and 5(b)], $\alpha = 1.5$ [Figs. 5(c) and 5(d)], and $\alpha = 2$ [Figs. 5(e) and 5(f)]. The dispersion curves for the real [Figs. 5(a), 5(c), and 5(e)] and the imaginary [Figs. 5(b), 5(d), and 5(f)] parts of the eigenvalues demonstrate the typical behavior for the wave instability [8,27]. Note also that as α decreases, so does the range of the wave number k of the curves related to the real parts of the eigenvalues.

As discussed before, the value of a_w must be smaller than a_H. This implies that there must exist a maximum value of the inertial time τ satisfying

$$a_w(\tau_{\max}) = a_H, \tag{49}$$

in order for a wave instability to occur in the hyperbolic fractional system (1). Figure 6 shows both sides of the equation $a_w = a_H$ as a function of the inertial time τ. The graph clearly demonstrates that there exists an inertial time $\tau_{\max}$ where wave instability and the Hopf instability coincide. For the parameter values $b = 2.5$, $c = 5$, and $d = 0.25$, we have analytically solved (49) and found that $\tau_{\max} = 3.6$.

V. NUMERICAL SIMULATIONS

This section will be devoted to the numerical confirmation of the validity of the analytical results obtained in the previous sections. To that end, we will describe first the computational approach followed here. Throughout, we will set a two-dimensional spatial domain $\Omega = [0,L] \times [0,L] \subseteq \mathbb{R}^2$ with $L \in \mathbb{R}^+$ and we let $T_0 \in \mathbb{R}^+$ represent some instant of time.

Under the assumptions of Sec. II, the Weyl fractional Laplacian operators of (1) can be represented as

$$\nabla^\alpha w = \nabla_x^\alpha w + \nabla_y^\alpha w, \tag{50}$$

where

$$\nabla_z^\alpha w = -c_\alpha\left({}_{-\infty}D_z^\alpha w + {}_z D_{+\infty}^\alpha w\right). \tag{51}$$

Here w represents u or v, and z denotes x or y. The constant c_α is as in (3) and we observe the following definitions (see [28] for a justification):

$$ {}_{-\infty}D_x^\alpha w = \frac{1}{\Gamma(2-\alpha)}\frac{\partial^2}{\partial x^2}\int_{-\infty}^x \frac{w(\zeta,y,t)}{(x-\zeta)^{\alpha-1}}d\zeta, \tag{52}$$

$$ {}_xD_{+\infty}^\alpha w = \frac{1}{\Gamma(2-\alpha)}\frac{\partial^2}{\partial x^2}\int_x^{+\infty} \frac{w(\zeta,y,t)}{(\zeta-x)^{\alpha-1}}d\zeta, \tag{53}$$

$$ {}_{-\infty}D_y^\alpha w = \frac{1}{\Gamma(2-\alpha)}\frac{\partial^2}{\partial y^2}\int_{-\infty}^y \frac{w(x,\zeta,t)}{(y-\zeta)^{\alpha-1}}d\zeta, \tag{54}$$

$$ {}_yD_{+\infty}^\alpha w = \frac{1}{\Gamma(2-\alpha)}\frac{\partial^2}{\partial y^2}\int_y^{+\infty} \frac{w(x,\zeta,t)}{(\zeta-y)^{\alpha-1}}d\zeta. \tag{55}$$

With these conventions, the problem under study in this section is described by the initial-value problem

$$\tau_u\frac{\partial^2 u}{\partial t^2} + \frac{\partial u}{\partial t} = u - av + buv - u^3 + \nabla^\alpha u,$$
$$\tau_v\frac{\partial^2 v}{\partial t^2} + \frac{\partial v}{\partial t} = u - cv + d\nabla^\beta v$$

such that

$$\begin{aligned} u(\mathbf{r},0) &= \phi(\mathbf{r}), \quad \mathbf{r} \in \Omega \\ v(\mathbf{r},0) &= \varphi(\mathbf{r}), \quad \mathbf{r} \in \Omega \\ \frac{\partial u}{\partial t}(\mathbf{r},0) &= \chi(\mathbf{r}), \quad \mathbf{r} \in \Omega \\ \frac{\partial v}{\partial t}(\mathbf{r},0) &= \psi(\mathbf{r}), \quad \mathbf{r} \in \Omega. \end{aligned} \tag{56}$$

Here $1 \leqslant \alpha \leqslant \beta$ and $1 \leqslant \beta \leqslant 2$. Obviously, this system is a more general form of (1). The functions ϕ and φ denote the initial profiles for u and v, respectively, and χ and ψ are the respective initial velocities. For simulation purposes, the functions ϕ and φ will be provided by suitable nonuniform perturbations. Meanwhile, the functions χ and ψ will be identically equal to zero.

The method used in this work to produce simulations is a finite-difference discretization of (56) using fractional centered differences [29]. To that end, we fix uniform partitions

$$0 = x_0 < x_1 < \cdots < x_M = L, \tag{57}$$

$$0 = y_0 < y_2 < \cdots < y_N = L \tag{58}$$

of $[0,L]$, for which the step sizes are $\Delta x = L/M$ and $\Delta y = L/N$, respectively. Consider a regular partition

$$0 = t_0 < t_1 < \cdots < t_K = T \tag{59}$$

of $[0,T_0]$ with norm $\Delta t = T/K$. We use $U_{m,n}^k$ and $V_{m,n}^k$ to denote numerical approximations of u and v, respectively, at the point $\mathbf{r}_{m,n} = (x_m, y_n)$ and time $t = t_k$. Moreover, we will employ the following discrete operators which are defined for any grid function W:

$$\delta_t W_{m,n}^k = \frac{W_{m,n}^{k+1} - W_{m,n}^k}{\Delta t}, \tag{60}$$

$$\delta_t^{(1)} W_{m,n}^k = \frac{W_{m,n}^{k+1} - W_{m,n}^{k-1}}{2\Delta t}, \tag{61}$$

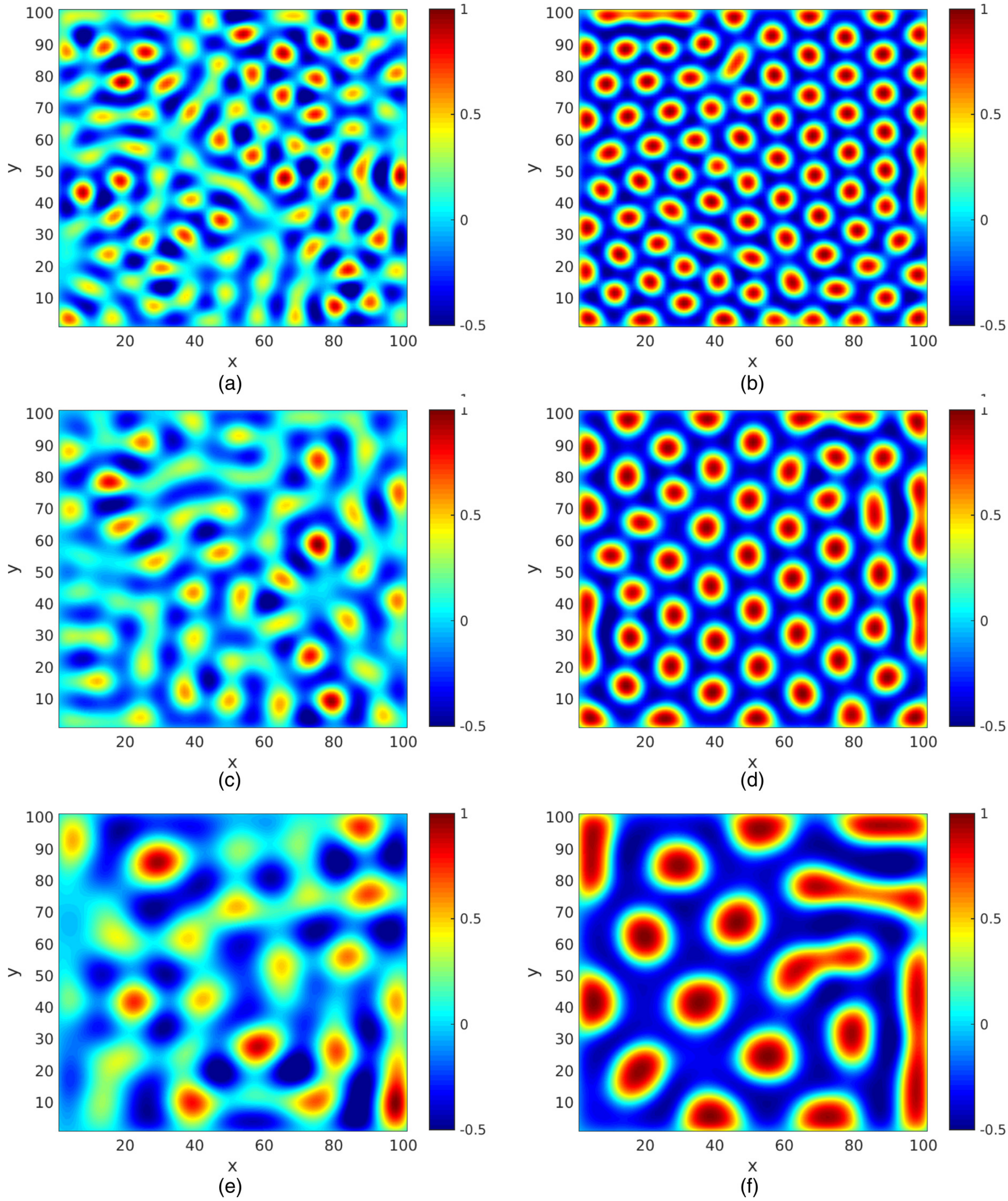

FIG. 7. Snapshots of the approximate solutions of the variable u of (56) versus x and y for (a) and (b) $\alpha = 2$, (c) and (d) $\alpha = 1.5$, and (e) and (f) $\alpha = 1$. The times (a), (c), and (e) $t = 100$ and (b), (d), and (f) $t = 1000$ were used in these simulations, together with the parameter values $c = 5$, $b = 2.5$, $d = 0.25$, and $\tau = 1$. Computationally, we used the method (69) with the numerical constants $L = 100$, $\Delta x = \Delta y = 1$, and $\Delta t = 0.01$. The graphs were normalized with respect to the absolute maximum of the solution at each time.

$$\delta_t^{(2)} W_{m,n}^k = \frac{W_{m,n}^{k+1} - 2W_{m,n}^k + W_{m,n}^{k-1}}{(\Delta t)^2}. \tag{62}$$

The first operators provide consistent approximations for the derivative of W with respect to t at the point $\mathbf{r}_{m,n}$ and time $t = t_k$, while the last approximates the second-order partial derivative of W with respect to t.

On the other hand, for each $1 \leqslant \alpha \leqslant 2$ and $k \in \mathbb{Z}$, let

$$g_k^{(\alpha)} = \frac{(-1)^k \Gamma(\alpha + 1)}{\Gamma(\frac{\alpha}{2} - k + 1)\Gamma(\frac{\alpha}{2} + k + 1)}. \tag{63}$$

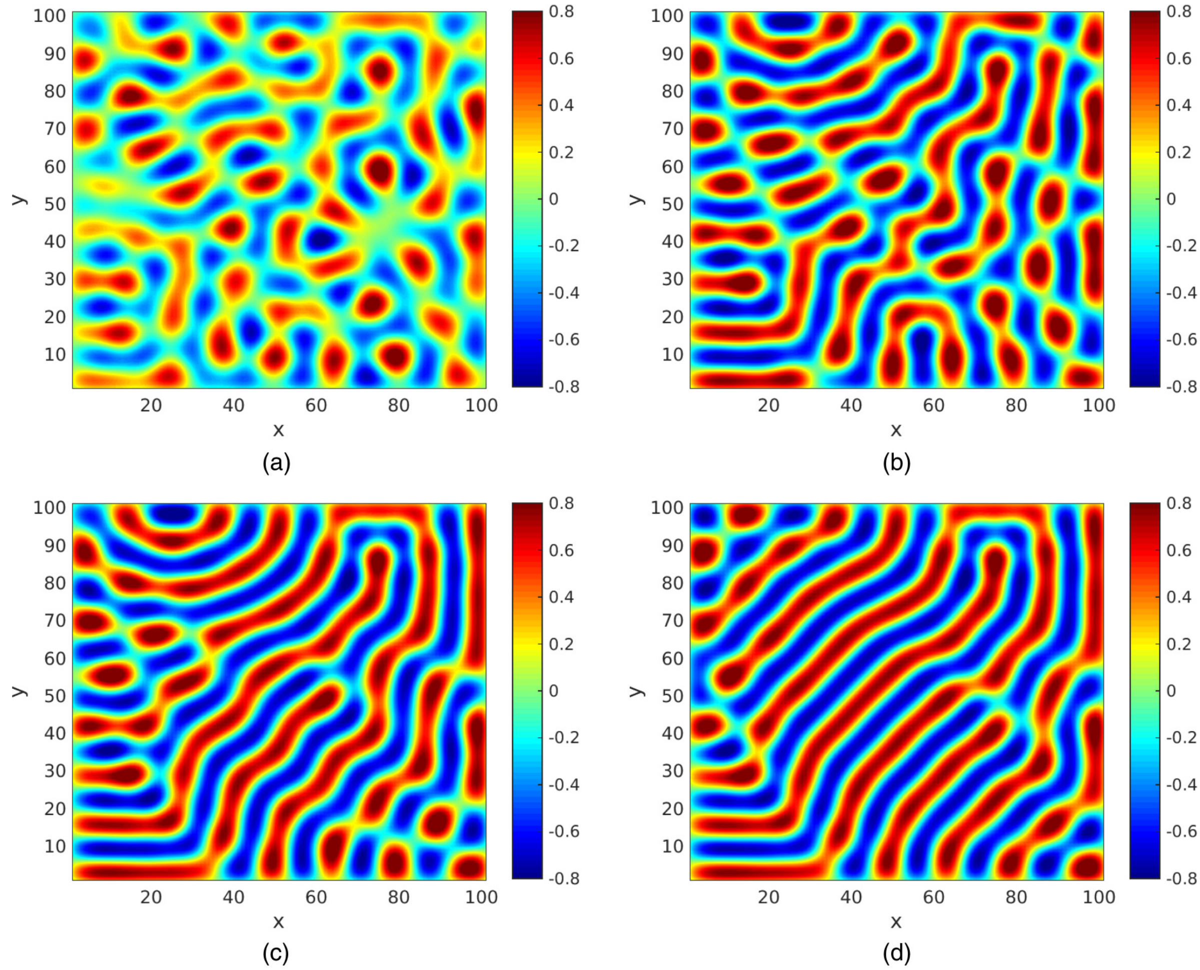

FIG. 8. Snapshots of the approximate solutions of the variable u of (56) versus x and y for $\alpha = \beta = 1.5$. The times (a) $t = 150$, (b) $t = 450$, (c) $t = 1000$, and (d) $t = 2000$ were used in these simulations, together with the parameter values $a = 7.45$, $b = 0.5$, $c = 5$, $d = 20$, and $\tau = 1$. Computationally, we used the method (69) with the numerical constants $L = 100$, $\Delta x = \Delta y = 1$, and $\Delta t = 0.01$. The graphs were normalized with respect to the absolute maximum of the solution at each time.

We define the linear operators

$$\delta_x^{(\alpha)} W_{m,n}^k = -\frac{1}{(\Delta x)^\alpha} \sum_{j=0}^{M} g_{m-j}^{(\alpha)} W_{j,n}^k, \tag{64}$$

$$\delta_y^{(\alpha)} W_{m,n}^k = -\frac{1}{(\Delta y)^\alpha} \sum_{j=0}^{N} g_{n-j}^{(\alpha)} W_{m,j}^k. \tag{65}$$

These operators provide consistent approximations of the partial derivatives of order α of W with respect to x and y, respectively [30]. Moreover, the two-dimensional fractional Laplacian of order α is approximated by

$$\delta_{\mathbf{r}}^{(\alpha)} W_{m,n}^k = \delta_x^{(\alpha)} W_{m,n}^k + \delta_y^{(\alpha)} W_{m,n}^k. \tag{66}$$

In the following, we will convey that

$$f_{m,n}^k = U_{m,n}^k - aV_{m,n}^k + bU_{m,n}^k V_{m,n}^k - \left(U_{m,n}^k\right)^3, \tag{67}$$

$$g_{m,n}^k = U_{m,n}^k - cV_{m,n}^k. \tag{68}$$

With this nomenclature, the method employed here to approximate the solutions of (56) is given by

$$\begin{aligned} \tau_u \delta_t^{(2)} U_{m,n}^k + \delta_t^{(1)} U_{m,n}^k &= f_{m,n}^k + \delta_{\mathbf{r}}^{(\alpha)} U_{m,n}^k, \\ \tau_u \delta_t^{(2)} V_{m,n}^k + \delta_t^{(1)} V_{m,n}^k &= g_{m,n}^k + \delta_{\mathbf{r}}^{(\beta)} V_{m,n}^k, \end{aligned}$$

such that

$$\begin{aligned} U_{m,n}^0 &= \phi(\mathbf{r}_{m,n}), \quad \mathbf{r}_{m,n} \in \Omega \\ V_{m,n}^k &= \varphi(\mathbf{r}_{m,n}), \quad \mathbf{r}_{m,n} \in \Omega \\ \delta_t U_{m,n}^0 &= \chi(\mathbf{r}_{m,n}), \quad \mathbf{r}_{m,n} \in \Omega \\ \delta_t V_{m,n}^0 &= \psi(\mathbf{r}_{m,n}), \quad \mathbf{r}_{m,n} \in \Omega. \end{aligned} \tag{69}$$

The methodology is an explicit technique which has a second-order local truncation error. It is worth pointing out that there exist other numerical methods available in the literature with higher orders of consistency. However, we have chosen this technique because it is relatively faster than other computational approaches. This is an important feature since all the numerical methods for fractional systems require a substantial amount of computer time and resources.

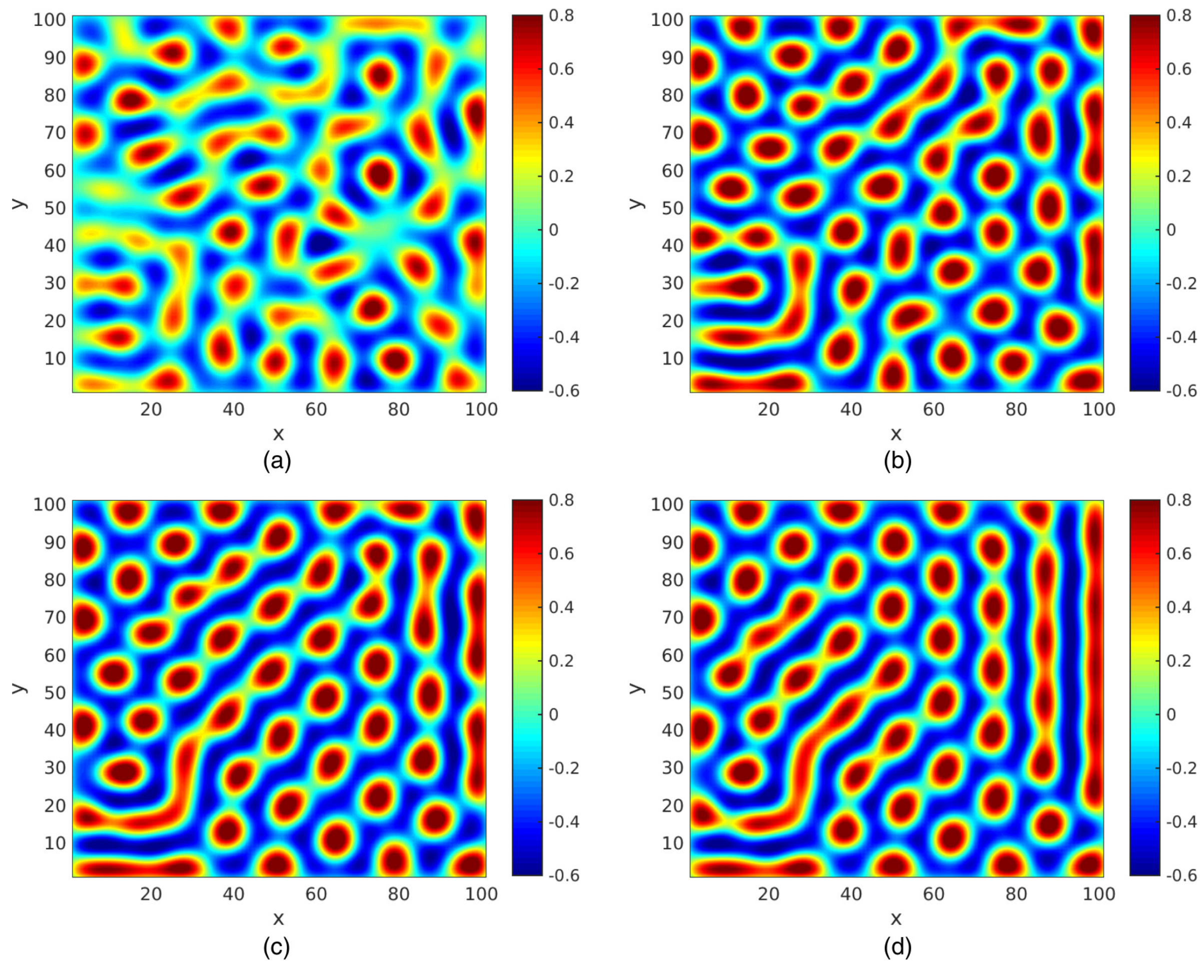

FIG. 9. Snapshots of the approximate solutions of the variable u of (56) versus x and y for $\alpha = \beta = 1.5$. The times (a) $t = 150$, (b) $t = 450$, (c) $t = 1000$, and (d) $t = 2000$ were used in these simulations, together with the parameter values $a = 7.45$, $b = 1.5$, $c = 5$, $d = 20$, and $\tau = 1$. Computationally, we used the method (69) with the numerical constants $L = 100$, $\Delta x = \Delta y = 1$, and $\Delta t = 0.01$. The graphs were normalized with respect to the absolute maximum of the solution at each time.

We provide now some simulations as evidence of the analytical predictions derived in the previous sections.

Example 1. Consider the system (56) with the parameter values $c = 5$, $b = 2.5$, $d = 0.25$, and $\tau = 1$. Computationally, let $L = 100$, $\Delta x = \Delta y = 1$, and $\Delta t = 0.01$. As initial profiles, let $U^0_{m,n}$ and $V^0_{m,n}$ be samples of a uniformly distributed random variable on the interval $[-0.03, 0.03]$ for each $\mathbf{r}_{m,n} \in \Omega$, and let $\chi = \psi \equiv 0$. Figure 7 shows snapshots of the approximate solutions of the variable u of (56) for various values of $\alpha = \beta$ and different times. Concretely, we used $\alpha = 2$ [Figs. 7(a) and 7(b)], $\alpha = 1.5$ [Figs. 7(c) and 7(d)], and $\alpha = 1$ [Figs. 7(e) and 7(f)], together with the times $t = 100$ [Figs. 7(a), 7(c), and 7(e)] and $t = 1000$ [Figs. 7(b), 7(d), and 7(f)]. These simulations confirm the fact that the wave number of Turing patterns increases as the order of differentiation α increases, in agreement with our analytical results. ■

Example 2. Let $b = 0.5$ and consider all the other parameter values as in Example 1. Figure 8 shows snapshots of the approximate solutions of the variable u of (56) versus x and y for $\alpha = \beta = 1.5$. The times $t = 150$ [Fig. 8(a)], $t = 450$ [Fig. 8(b)], $t = 1000$ [Fig. 8(c)], and $t = 2000$ [Fig. 8(d)] were used in these simulations and the graphs have been normalized with respect to the absolute maximum of the solution at each time. In this case, the solution first breaks up into hexagons due to the small perturbations at the initial time. The emergent hexagons are not stable and they are replaced gradually by stripes. Eventually, the stripes prevail over the whole domain and the qualitative dynamics of the system does not undergo any further substantial changes. This is in agreement with the analytical results and with the parabolic scenario. ■

Example 3. Set now $b = 1.5$ and consider the same parameter values as in Example 2. Under these circumstances, Fig. 9 shows snapshots of the approximate solutions of the variable u of (56) versus x and y. We employed $\alpha = \beta = 1.5$ and the times $t = 150$ [Fig. 9(a)], $t = 450$ [Fig. 9(b)], $t = 1000$ [Fig. 9(c)], and $t = 2000$ [Fig. 9(d)]. Notice that the results show the coexistence of strips and hexagons at different times. Ultimately, both the hexagonal and the striped patterns coexist. ■

Example 4. Finally, let us set $b = 2.5$ and $\tau = 3$, while the remaining parameters are as in Example 2. Figure 10 shows snapshots of the approximate solutions of the variable u of (56) versus x and y at the times $t = 150$ [Fig. 10(a)], $t = 450$ [Fig. 10(b)], $t = 1000$ [Fig. 10(c)], and

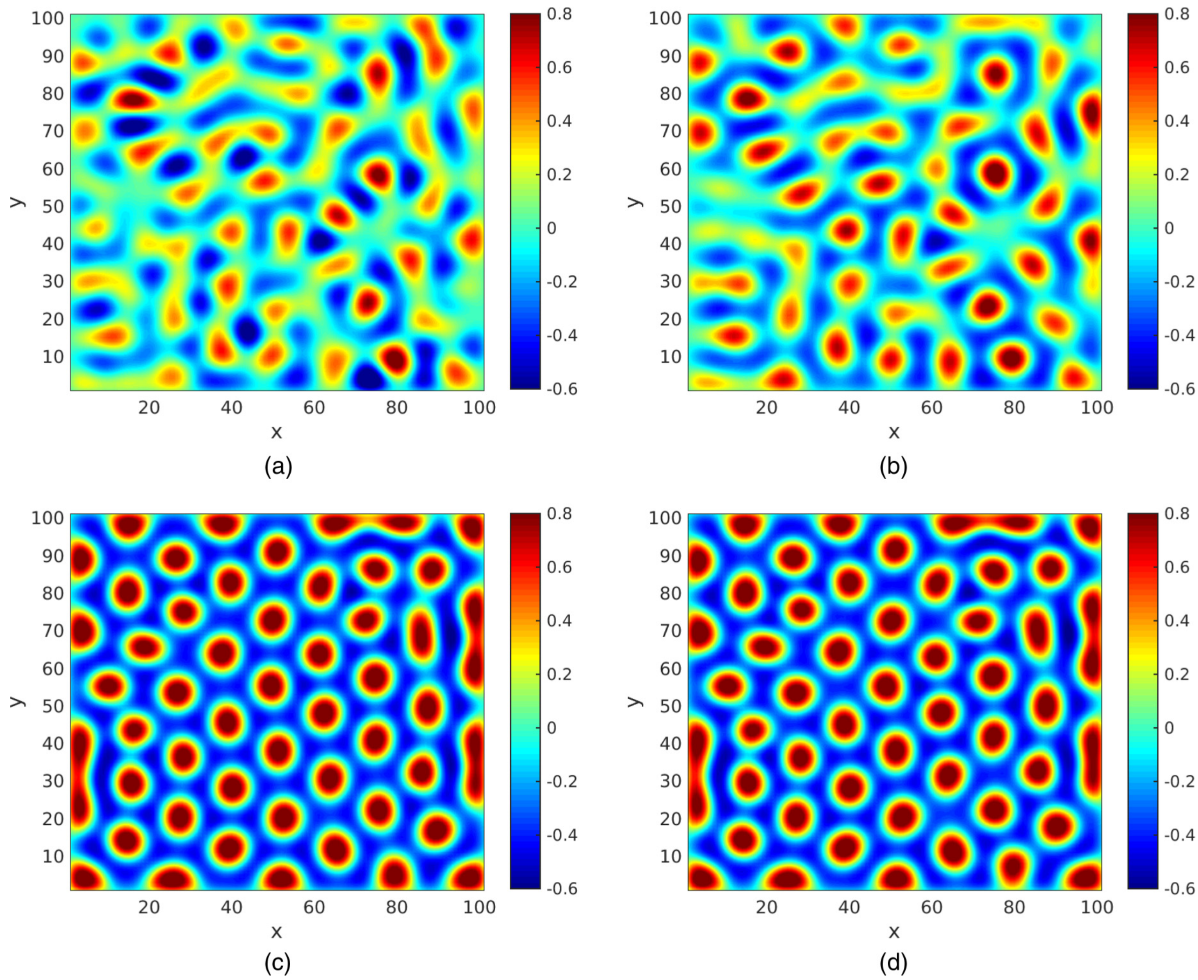

FIG. 10. Snapshots of the approximate solutions of the variable u of (56) versus x and y for $\alpha = \beta = 1.5$. The times (a) $t = 50$, (b) $t = 150$, (c) $t = 450$, and (d) $t = 1000$ were used in these simulations, together with the parameter values $a = 7.45$, $b = 2.5$, $c = 5$, $d = 20$, and $\tau = 3.5$. Computationally, we used the method (69) with the numerical constants $L = 100$, $\Delta x = \Delta y = 1$, and $\Delta t = 0.01$. The graphs were normalized with respect to the absolute maximum of the solution at each time.

(d) $t = 2000$ [Fig. 10(d)]. In our simulations, we noted the presence of stable hexagonal patterns at different times. Moreover, the pattern dynamics converges to stable hexagonal patterns. ■

VI. CONCLUSION

In this work we investigated the analytic aspects of wave instabilities in hyperbolic reaction-diffusion systems. We introduced Weyl fractional operators in our system to describe species undergoing anomalous superdiffusion. Inertial terms were introduced in the model studied in [15] and a linear stability analysis was performed. The results revealed that the superdiffusive exponent α and the inertial time τ strongly influence the wave number of Hopf wave bifurcations, whereas the Turing wave number is independent of τ. We showed that the maximum value of the inertial time for a wave instability to occur in our hyperbolic fractional system is $\tau_{\max} = 3.6$. Some numerical simulations were performed to show qualitatively the validity of the analytical predictions obtained in this work.

Before closing this work it is important to point out the essential features of this study with respect to some recent works available in the literature [15,16]. To start with, those papers only investigated conditions that guarantee the presence of Turing instabilities. In the present paper we investigated both Turing and wave instabilities. In order to understand the effects of initial conditions, we extended the models investigated in those works to the anomalously diffusive hyperbolic scenario. This approach has the virtue of describing transport phenomena with inertia. From that perspective, a wide range of phenomena in biology, physics, and chemistry are modeled by the present fractional system and relevant applications to these areas may be proposed [20].

ACKNOWLEDGMENTS

The authors would like to thank the anonymous reviewers for all their invaluable comments and criticisms. One of us (A.M.) acknowledges fruitful discussions with Prof. K. Showalter of the University of West Virginia. He also acknowledges the invitation and financial support from the Abdus Salam International Centre for Theoretical Physics.

[1] V. Mendez, S. Fedotov, and W. Horsthemke, *Reaction-Transport Systems: Mesoscopic Foundations, Fronts, and Spatial Instabilities*, 1st ed. (Springer Science + Business Media, Heidelberg, 2010).
[2] V. Méndez, D. Campos, and W. Horsthemke, Phys. Rev. E **90**, 042114 (2014).
[3] G. Abramson, A. R. Bishop, and V. M. Kenkre, Phys. Rev. E **64**, 066615 (2001).
[4] K. K. Manne, A. J. Hurd, and V. M. Kenkre, Phys. Rev. E **61**, 4177 (2000).
[5] E. P. Zemskov, M. A. Tsyganov, and W. Horsthemke, Phys. Rev. E **91**, 062917 (2015).
[6] W. Horsthemke, in *Noise in Complex Systems and Stochastic Dynamics III*, edited by L. B. Kish, K. Lindenberg, and Z. Gingl, SPIE Proc. Vol. 5845 (SPIE, Bellingham, 2005), pp. 12–27.
[7] W. Horsthemke, Phys. Rev. E **60**, 2651 (1999).
[8] E. P. Zemskov and W. Horsthemke, Phys. Rev. E **93**, 032211 (2016).
[9] G. Hornung, B. Berkowitz, and N. Barkai, Phys. Rev. E **72**, 041916 (2005).
[10] D. del Castillo-Negrete, B. Carreras, and V. Lynch, Phys. Plasmas **11**, 3854 (2004).
[11] R. Metzler and J. Klafter, Phys. Rep. **339**, 1 (2000).
[12] G. M. Zaslavsky, Phys. Rep. **371**, 461 (2002).
[13] R. Metzler and J. Klafter, J. Phys. A: Math. Gen. **37**, R161 (2004).
[14] A. A. Golovin, B. J. Matkowsky, and V. A. Volpert, SIAM J. Appl. Math. **69**, 251 (2008).
[15] L. Zhang and C. Tian, Phys. Rev. E **90**, 062915 (2014).
[16] V. Dufiet and J. Boissonade, Phys. Rev. E **53**, 4883 (1996).
[17] H. Teimouri, B. Bozorgui, and A. B. Kolomeisky, J. Phys. Chem. B **120**, 2745 (2016).
[18] P. V. Kuptsov, S. P. Kuznetsov, and A. Pikovsky, Phys. Rev. Lett. **108**, 194101 (2012).
[19] R. Zillmer and A. Pikovsky, Phys. Rev. E **67**, 061117 (2003).
[20] J. Shin, A. G. Cherstvy, W. K. Kim, and R. Metzler, New J. Phys. **17**, 113008 (2015).
[21] F. Riewe, Phys. Rev. E **55**, 3581 (1997).
[22] V. Dufiet and J. Boissonade, J. Chem. Phys. **96**, 664 (1992).
[23] V. Dufiet and J. Boissonade, Physica A **188**, 158 (1992).
[24] J. Verdasca, A. De Wit, G. Dewel, and P. Borckmans, Phys. Lett. A **168**, 194 (1992).
[25] M. C. Cross and P. C. Hohenberg, Rev. Mod. Phys. **65**, 851 (1993).
[26] X.-C. Zhang, G.-Q. Sun, and Z. Jin, Phys. Rev. E **85**, 021924 (2012).
[27] A. M. Zhabotinsky, M. Dolnik, and I. R. Epstein, J. Chem. Phys. **103**, 10306 (1995).
[28] V. E. Tarasov, J. Phys. A: Math. Gen. **39**, 14895 (2006).
[29] M. D. Ortigueira, Int. J. Math. Math. Sci. **2006**, 48391 (2006).
[30] X. Wang, F. Liu, and X. Chen, Adv. Math. Phys. **2015**, 590435 (2015).